

Characterization of indium hydroxide powders synthesized by a precipitation method

Won-Jun Lee^{a,b}, Eun-Kyoung Choi^{a,b}, Ung-Soo Kim^a, Jong-Young Kim^a, Kwang-Bo Shim^c, Hae-Jin Hwang^b and Woo-Seok Cho^{a,*},

^aIcheon Branch, Korea Institute of Ceramic Engineering & Technology (KICET), Icheon 17303, Korea

^bSchool of Material Science and Engineering, Inha University, Incheon 22212, Korea

^cDepartment of Materials Science and Engineering, Hanyang University, Seoul 04763, Korea

Indium hydroxide powders were synthesized using indium nitride, and the characteristics of the indium hydroxide powder were investigated according to the precipitate aging time and the pH and concentration of the liquid synthesis medium. Indium hydroxide (In(OH)₃) and indium oxide hydroxide (InOOH) phases co-existed in all conditions studied here. The crystallite size of In(OH)₃ was more dependent on the concentration and pH of the reaction medium compared to that of InOOH. Hence, the relative crystallite scale of In(OH)₃ increased with increasing concentration and pH of the reaction liquid more than that of InOOH. Although the crystallite size did not change much with an increase of precipitate aging time, the specific surface area decreased greatly. Such results can aid in the synthesis of indium oxide particles that are used for producing ITO targets.

Key words: Indium hydroxide, Indium oxide hydroxide, Precipitation, Raw material.

Introduction

Transparent conduction oxides (TCO) are core materials in the display industry. Indium tin oxide (ITO) is a representative TCO material, with a bandgap > 3.5 eV and high electrical conductivity. One of its most important material properties is its high light transmission (> 85%) within the visible spectrum [1-3]. As such, ITO is not only used in pixel electrodes or common electrodes in flat displays including organic light emitting diode and liquid crystal displays, but also in other areas like liquid crystal cells, gas sensors and solar cells [3-6].

ITO electrodes can be manufactured in a variety of ways, including chemical vapor deposition (CVD), spraying, thermal deposition, ion plating and sputtering [7-10]. Among these methods, sputtering processing is the most common for uniformly coating large surface areas and for obtaining high-quality films. However, when an ITO target is used for long-term sputtering, impurities known as nodules form on the surface of the ITO target, which can reduce the deposition rate of transparent electrode films and act as surface defects [11-12]. Nodules are also often created by local arcing when using high applied voltage within high vacuum sputtering equipment. The high density of the ITO

target increases the cooling effectiveness for cooling the heat generated during sputtering, reducing the electric resistance of the ITO target as a result. For this reason, the formation of nodules can be suppressed by controlling the arcing phenomenon. Thus, an ITO target with high sintered density needs to be developed. In order to obtain high density ITO targets, various methods such as pressure sintering, hot pressing (HP), and hot isostatic pressing (HIP) can be used [13, 14]. For HP and HIP however, equipment costs are high and both methods have difficulty in mass-producing large targets, making them not suitable for mass production. Currently, ITO targets are produced by a general sintering method under atmospheric pressure using nano-scale powders with high sinterability. ITO does not sinter easily, and in some cases a small amount of sintering aid is added to increase sinterability [15]. However, since high electrical conductivity requires > 99.99% purity, using additives to improve sinterability is not a viable strategy. The nano-scale indium oxide powder used in ITO target production is normally produced by precipitation methods, which can easily realize mass production. First, indium metal is dissolved using nitric acid (HNO₃) and neutralized by ammonia water or ammonia gas to obtain indium hydroxide powder. Indium oxide powder can then be obtained by heat processing the obtained indium hydroxide powder. Hence, the characteristics of indium oxide powder are largely influenced by those of the precursor indium hydroxide powder, which have not yet been studied in detail.

*Corresponding author:
Tel : +82-31-645-1405
Fax: +82-31-645-1486
E-mail: wscho@kicet.re.kr

In this study, indium hydroxide powder was synthesized by a precipitation method, which can easily realize mass production with high purity above 99.99%. The purpose of the study is to determine the characteristics of precipitates obtained after changing the precipitation processing variables including pH, concentration and aging time, and to study the formation behavior of indium hydroxide powder.

Experimental

Synthetic process

Indium metal (In, 99.99%, Top Material) was used to synthesize indium hydroxide and nitric acid (HNO₃, Dongwoo fine-chemical, 60%, electronic grade, Korea) was used as the solvent to produce an indium nitride solution. Ammonia water (NH₄OH) was used to obtain precipitates in the range of pH 5-9.

Indium nitride solutions were prepared at 0.2, 0.4, 0.6 and 0.8 M by dissolving indium metal in nitric acid solution. For each produced indium nitride solution, ammonia water was added with a rate of 3 mL/min to obtain solutions with pH of 5, 6, 7, 8, and 9, and the precipitate appeared as a white solid. To observe the aging effects of the precipitates, the aging time was varied within the range of 0-40 hrs. A centrifuge was used to process the gel type precipitate, which was dried in an oven for 24 hrs. The powder cohered during drying and was pulverized using agate induction.

Characterization

X-ray diffraction (XRD, Rigaku, D/2500VL/PC, (Cu K α (λ = 1.5402 nm)) was used in order to confirm the crystal type and crystallite size of the processed precipitates. In addition, the Scherrer equation (equation (1)) was used to calculate the crystallite size

$$\tau = \frac{K\lambda}{\beta \cos \theta} \quad (1)$$

where β is the full width at half maximum (FWHM), K is the shape factor, λ is the wavelength (CuK α_1 = 1.54056 Å), and τ is the crystallite size. Transmission electron microscopy (TEM, JEM-2100F, 200 kV, JEOL, Japan) was used to confirm the shape, size, and lattice characteristics of the particles. The specific surface area (Brunauer-Emett-Teller (BET), Micromerics Tristar II, Instrument Co., Norcross, GA, USA) of the produced indium hydroxide powder was also measured.

Result and Discussion

Fig. 1 shows the XRD patterns of the precipitates produced at 0.2-0.8 M and at pH of 5-9, analyzing the crystal structure behavior according to changes in concentration and pH. In all conditions, the In(OH)₃ phase (JCPDS No. 71-2194) and indium oxide hydroxide (InOOH) phase (JCPDS No.71-2276) co-existed [16]. Their crystal structures are cubic and orthorhombic respectively, and the FWHM value of the XRD peaks corresponding to In(OH)₃ phase was less than the FWHM value for the XRD peaks corresponding to indium oxide hydroxide.

Each crystallite size was calculated using equation (1) on the main peaks $2\theta = 22.2^\circ$ for In(OH)₃ and $2\theta = 25.8^\circ$ for InOOH (Fig. 2). The crystallite size of In(OH)₃ at pH 5-8 changed within a range of 9-16 nm, and gradually increased as the concentration of the indium nitride solution increased. On the other hand, there was almost no difference in crystallite size due to concentration changes for the powder synthesized at pH = 9. The crystallite size of InOOH had little dependence on changes of concentration and pH, and only showed small changes of 3-6 nm; minor increases were only observed at 0.2 M. Considering these, the increase in crystallite size of In(OH)₃ depends on concentration and pH moreso than in InOOH.

Fig. 3 shows the derived results of the integrated area

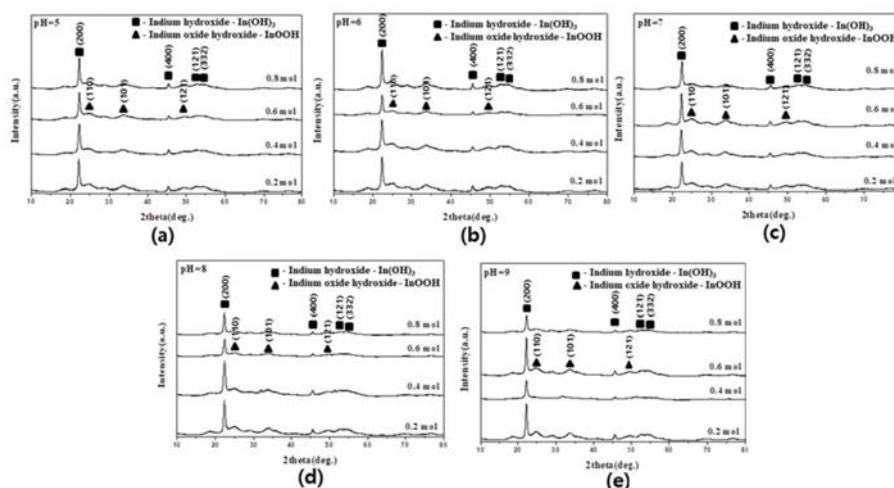


Fig. 1. XRD patterns of powders obtained at pH (a) 5, (b) 6, (c) 7, (d) 8 and (e) 9.

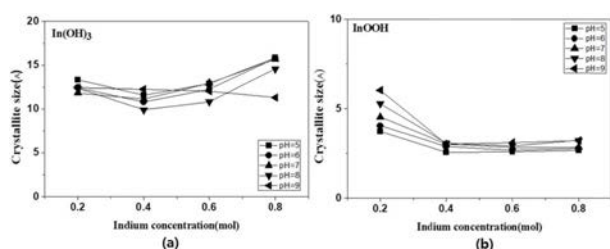


Fig. 2. Changes of crystallite sizes of (a) indium hydroxide and (b) indium oxide hydroxide calculated using equation (1).

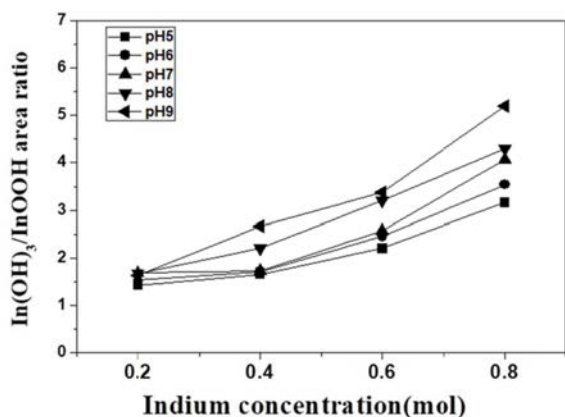


Fig. 3. Integral area ratio of $\text{In}(\text{OH})_3/\text{InOOH}$ in the XRD patterns of samples obtained at pH = 5-9.

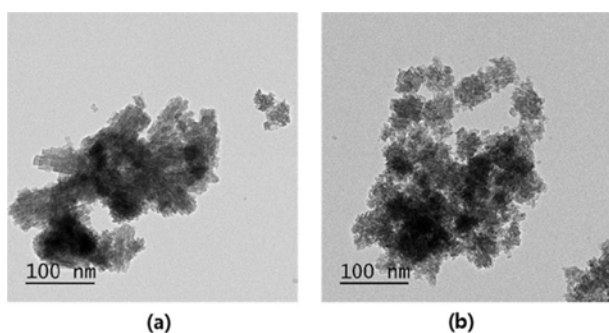


Fig. 4. Low magnification TEM images of (a) indium hydroxide and (b) indium oxide hydroxide produced at (a) concentration=0.8 M, pH = 9; (b) concentration = 0.2 M, pH = 5.

ratio of XRD peaks corresponding to $\text{In}(\text{OH})_3$ and InOOH based on increases in concentration. As the concentration increased, the ratio of $\text{In}(\text{OH})_3$ to InOOH also increased, and increasing the pH increased the ratio of $\text{In}(\text{OH})_3$. The above results can be correlated to a pH solubility curve; as the pH increases, the concentration increases as more OH^- is generated as In^{3+} , $\text{In}(\text{OH})^{2+}$, $\text{In}(\text{OH})_2^+$, $\text{In}(\text{OH})_3$, and $\text{In}(\text{OH})_4^-$ in the solution [17]. It is suspected that, because pH 5-8 is the stable region for $\text{In}(\text{OH})_3$ and increasing the indium concentration stimulates the formation of $\text{In}(\text{OH})_3$, the crystallite size increases as a result. However, $\text{In}(\text{OH})_3$ and $\text{In}(\text{OH})_4^-$ co-exist at pH > 8 and the amount of $\text{In}(\text{OH})_4^-$ present increases as the pH increases [17]. Therefore, the increase of indium concentration at pH = 9 seems to contribute to the generation of $\text{In}(\text{OH})_4^-$,

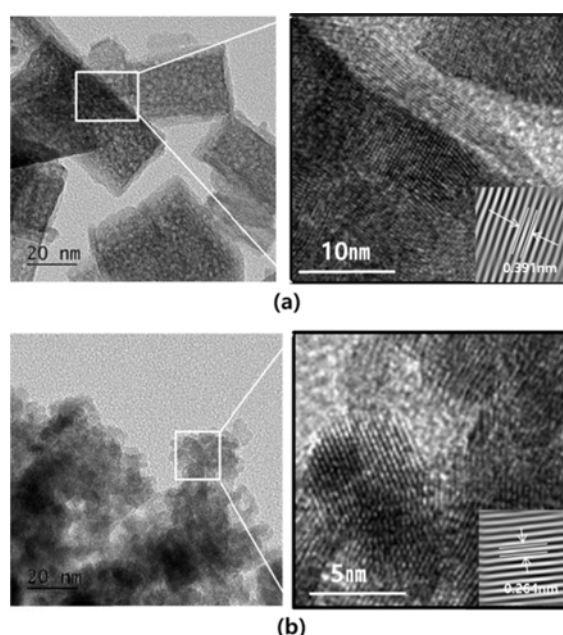


Fig. 5. High magnification TEM image of (a) indium hydroxide and (b) indium oxide hydroxide produced at (a) concentration=0.8 M, pH = 9; (b) concentration = 0.2 M, pH = 5.

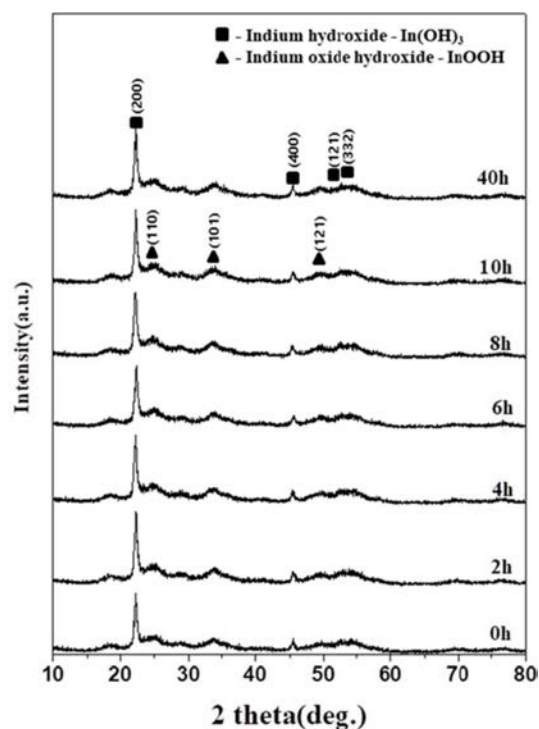


Fig. 6. XRD patterns of indium hydroxides obtained at different aging times.

while the crystallite size hardly changes. Moreover, it is expected that the formation of InOOH is most closely related to $\text{In}(\text{OH})_2^+$ among all ion species. $\text{In}(\text{OH})_2^+$ ions are suspected to generate InOOH precipitates by reacting with O_2 . Although the amount of $\text{In}(\text{OH})_2^+$ present is much smaller than that of $\text{In}(\text{OH})_3$, its formation is promoted as the concentration of indium and the

solution pH decrease [17]. Therefore, as the indium concentration and solution pH increase, the phase ratio of $\text{In}(\text{OH})_3$ is estimated to increase.

Fig. 4 shows TEM data of powders synthesized from two different solutions, one with concentration of 0.8 M and pH=9, and the other with 0.2 M concentration at pH=5. In both samples, two types of morphology appeared: a rectangular shape of approximately 25×60 nm and a circular particle 3-5 nm in diameter. The size of the circular particle matches the crystallite size of InOOH . However, the rectangular size does not match with the both the crystallite sizes of InOOH or $\text{In}(\text{OH})_3$. Magnified images of the rectangle and circular particle are shown in Fig. 5. The rectangle does not appear as a single crystal, but is rather composed of many single crystals and some non-crystalline species, where the size of a single crystal is approximately 15 nm. This size is almost identical to the crystallite size of $\text{In}(\text{OH})_3$. Lattice images were examined in order to further investigate the present phases. The lattice distance shown in Fig. 5(a) is 0.391 nm, which is identical to the d_{200} value of $\text{In}(\text{OH})_3$. Therefore, it is possible to determine that the rectangular particles are

polycrystalline $\text{In}(\text{OH})_3$. The lattice distance of the circular particles (5 nm diameter) was also investigated. As shown in Fig 5(b), the 0.264 nm distance here matches well with the d_{110} value of InOOH . Based on this, the circular shaped particles are single-crystal InOOH .

Fig. 6 shows XRD data for variable aging times of the precipitate, obtained by titrating liquid indium nitride solution (0.2 M) with ammonia water to pH = 7. The two morphologies mentioned above were present in all samples. Changes in the crystallite sizes due to precipitate aging time were not observed (Fig. 7). The crystallite size of $\text{In}(\text{OH})_3$ forms within a size range of 15.6-17.6 nm, and did not show any significant change according to aging time. Changes in the crystallite size of InOOH were also not clearly observed, and were only confirmed to change within a range of 2.5-4.3 nm. Such results coincides with other observations in our study.

Fig. 8 shows the specific surface area data of powders obtained at variable aging times. For the powder obtained with no solution aging, its specific surface area was $117.4 \text{ m}^2/\text{g}$, which decreased greatly to $108.7 \text{ m}^2/\text{g}$ after 4 hrs aging, and decreased slightly after the aging time increased further. As shown in Fig. 7, although the crystallite size did not change much, the specific surface area decreased greatly as the aging time increased (Fig. 8). For specific surface area to decrease without any increase in crystallite size, the indium hydroxide particle size must increase in size to a poly-crystal. Such results are an important factor in controlling the powder size when obtaining indium oxide powder by heat processing indium hydroxide. In order to determine the influence of aging time on the particle size behavior, TEM was used on powders obtained at aging times of 0-40 hrs for microstructure observations (Fig. 9). The un-aged powder had weaker cohesion and a smaller particle size than the powders at 40 hrs aging time (Fig. 9). The initial deposited materials are formed with very fine nano-scale particles, which are assumed to cause the unstable high surface energy state. This indicates that the particles

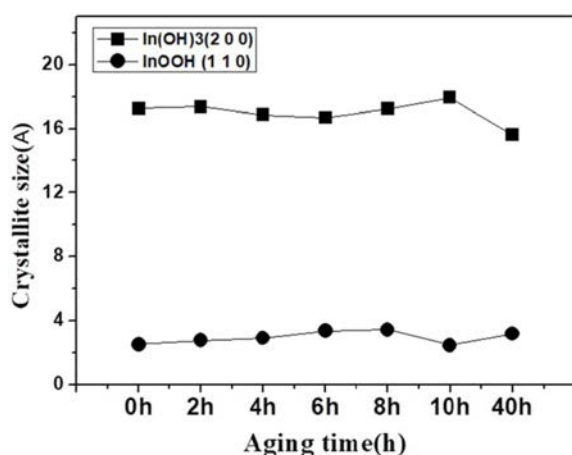


Fig. 7. Crystallite size and D values of samples with variable aging time (0.2 M, pH = 7).

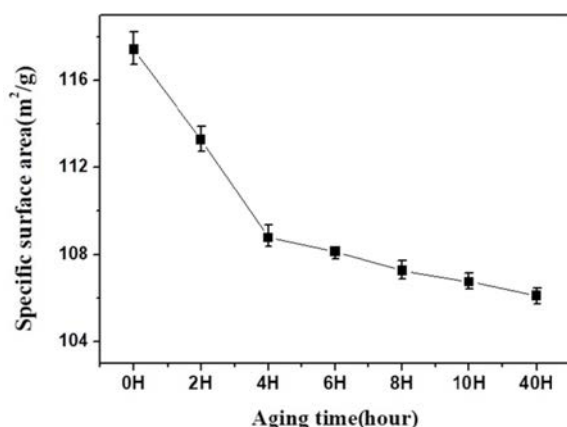


Fig. 8. BET specific surface areas of indium hydroxide prepared at different aging times (0-40 hrs).

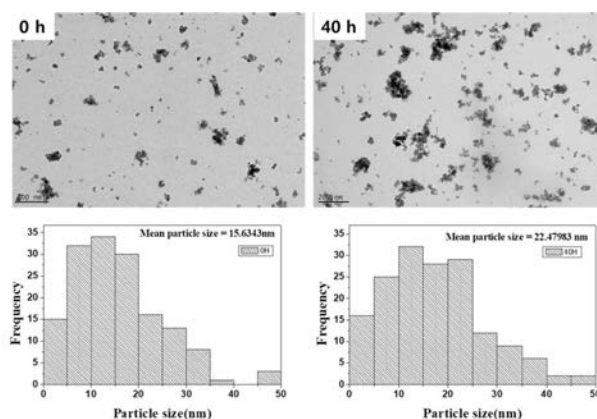


Fig. 9. TEM images and particle size distributions according to aging time (0 h, 40 hrs).

cohere more strongly to reduce the surface energy and increase the particle size as the aging time increases. Once these particles reach a certain size, no more cohesion takes place and the particle size remains more or less constant. Based on these results, the aging time influences the cohesion of indium hydroxide particles and the size of indium oxide particles when synthesizing indium oxide from indium hydroxide powder.

Conclusions

The characteristics of indium hydroxide powder were observed for indium hydroxide synthesized using indium nitride, based on solution pH, concentration, and precipitate aging time. Indium hydroxide ($\text{In}(\text{OH})_3$) and indium oxide hydroxide (InOOH) phases co-existed in all conditions measured here. At solution pH = 5-8, the crystallite size of $\text{In}(\text{OH})_3$ changed at 9-16 nm and gradually increased in size as the concentration of the indium nitride solution increased. On the other hand, change in crystallite size based on concentration changes were not observed for the powder synthesized at pH 9. The crystallite size of InOOH hardly depended on the solution concentration or pH, and only displayed minor changes within a range of approximately 3-6 nm. Considering such results, the crystallite size of the $\text{In}(\text{OH})_3$ phase depends on the concentration and pH more so than that of InOOH . Although the crystallite size of $\text{In}(\text{OH})_3$ did not change much according to the precipitates aging time, the specific surface area reduced greatly as the aging time increased. Such results can improve the size control of indium oxide particles that are used in producing ITO targets.

Acknowledgments

This work was supported by Infrastructure program

for New Value Creation of Traditional Ceramic Industry (BUS010025000) under Ministry of Trade, Industry and Energy.

References

1. N. Manavizadeh, F.A. Broumand, E.A. Soleimani, F. Raissi, S. Bagherzadeh, A. Khodayari, and M.A. Rasouli, *Thin Solid Films* 517 (2009) 2324-2327.
2. H.D. Jang, C.M. Seong, H.K. Chang, and H.C Kim, *Curr. Appl. Phys.* 6[6] (2006) 1044-1047.
3. K.L. Chopra, S. Major, and D.K. Pandya, *Thin Solid Films* 102 (1983) 43-46.
4. M.Y. Ryu, J.H. Choi, and H.T. Kim, *J. Korean Ind. Eng. Chem.* 12[3] (2001) 249-254.
5. H.L. Ma, D.H. Zhang, P. Ma, S.Z. Win, and S.Y. Li, *Thin Solid Films* 263(1995)105-110.
6. E.F. Keshenler, and G. Turgut, *J. Ceram. Proc. Res.* 17[12] (2016) 1254-1259.
7. Y. Djaoued, V.H. Phong, S. Badilescu, P.V. Ashrit, F.E. Girouard and V.V. Truong, *Thin Solid Films* 293 (1997) 108-112.
8. T. Furusaki, K. Kordaira, M. Yamamoto, S. Shimada, and T. Matsushita, *Mater. Res. Bull.* 21 (1986) 803-806.
9. T. Minami, *J. Vacc. Sci. & Technol.* A17 (1999) 1765-1772.
10. H.K. Jeoung, and K.M. Lee, *J. Ceram. Proc. Res.* 17[4] (2016) 281-285.
11. N. Kikuchi, E. Kusano, H. Nanto, A. Kinbara and H. Hosono, *Vacuum* 59[2-3] (2000) 492-499.
12. Y. Shigesato, R. Koshi-ishi, T. Kawashima and J. Ohsako, *Vacuum* 59[2-3] (2000) 614-621.
13. N. Nadaud, M. Nanot, and P. Boch, *J. Am. Ceram. Soc.* 77[3] (1994) 843-846.
14. T. Vojnovich, and R.J. Bratton, *J. Am. Ceram. Soc. Bull.* 54 (1975) 216-217.
15. J.S. Kim, K.W. Ryu, J.H. Koh, and Y.H. Lee, *J. Kor. Inst. Elec. Res.* (2007) 114-115.
16. Y. Luo, X. Zheng, L. Zou, S. Hu, and J. Yang, *ECS Solid State Letters* 4[7] (2015)2162-8742.
17. C.F. Baes Jr, R.E. Mesmer, in "Hydrolysis of cations" (Krieger Publishing Company Malabar Florida, 1976) p. 321-322.